



Spectral evolution of the X-ray nova XTE J1859+226 during its outburst observed by *BeppoSAX* and *RXTE*

R. Farinelli,^{1,2*} L. Amati,³ N. Shaposhnikov,⁴ F. Frontera,¹ N. Masetti,³ E. Palazzi,³ R. Landi,³ C. Lombardi,¹ M. Orlandini³ and C. Brocksopp⁵

¹Dipartimento di Fisica, Università di Ferrara, Via Saragat 1, I-44122 Ferrara, Italy

²INAF-IASF, Sezione di Palermo, Via U. La Malfa 153, I-90146 Palermo, Italy

³INAF-IASF, Sezione di Bologna, Via Gobetti 101, I-40129 Bologna, Italy

⁴NASA-GSFC, Astrophysics Science Division, Greenbelt, MD 20771, USA

⁵Mullard Space Science Laboratory, University College London, Holmbury St Mary, Dorking, Surrey RH5 6NT

Accepted 2012 October 23. Received 2012 October 4; in original form 2011 October 4

ABSTRACT

We report results of an extensive analysis of the X-ray nova XTE J1859+226 observed with *BeppoSAX* and the *Rossi X-ray Timing Explorer* during the 1999 source outburst. We modelled the source spectrum with a multicolour blackbody-like feature plus the generic Comptonization model BMC which has the advantage of providing spectral description of the emitted-radiation properties without assumptions on the underlying physical process. The multicolour component is attributed to the geometrically thin accretion disc, while the Comptonization spectrum is claimed to originate in the innermost sub-Keplerian region of the system (transition layer). We find that XTE J1859+226 covers all the spectral states typical of black hole sources during its evolution across the outburst; however, during the very high state, when the disc contribution to the total luminosity is more than 70 per cent and the root mean square variability $\lesssim 5$ per cent, the high-energy photon index is closer to a hard state value ($\Gamma \sim 1.8$). The BMC normalization and photon index Γ well correlate with the radio emission, and we also observed a possible saturation effect of Γ at the brightest radio emission levels. A strong positive correlation was found between the fractions of Comptonized seed photons and the integrated root mean square variability, which strengthens the idea that most of the fast variability in these systems is attributable to the innermost Compton cloud, which may be also identified as a jet.

Key words: accretion, accretion discs – radiative transfer – X-rays: individual: XTE J1859+226 – X-rays: binaries.

1 INTRODUCTION

X-ray novae, or soft X-ray transients (SXTs), are low-mass X-ray binaries which undergo a sudden and unpredictable increase in intensity up to two to six orders of magnitude in X-rays (Liu, van Paradijs & van den Heuvel 2001). These outbursts occur usually on time-scale of decades, even if there are cases like GX 339–4 where regular annual outbursts are seen (McClintock & Remillard 2006). Their light curves are characterized by a typical rise time of few days and an e-folding decay time of several tens of days. In these systems the accreting compact object is found to be a neutron star (NS) or a black hole (BH; e.g. Tanaka & Shibazaki 1996; Cherepashchuk 2000). During the outbursts, thought to be originated by a dramatic change in the mass accretion rate, the X-ray

spectrum evolves through different states, classified according to the presence and relative prominence of a soft thermal component and a hard tail component (e.g. Zdziarski & Gierliński 2004; Cadolle Bel et al. 2006; Remillard & McClintock 2006; Del Santo et al. 2008; Laurent et al. 2011). The thermal component is commonly thought to be generated in the inner regions of the accretion disc, and the non-thermal hard tail by Comptonization of the soft thermal photons by a hot electron corona (e.g. Poutanen & Svensson 1996). The X-ray spectra of several SXTs may allegedly show a reflection component and/or emission lines and edges, due to reprocessing of the hard X-ray photons by the cold outer regions of the accretion disc (e.g. Magdziarz & Zdziarski 1995). The power spectra derived from the X-ray light curve of SXTs in outburst are characterized by a red noise component with superimposed quasi-periodic oscillations (QPOs) at different and quickly varying frequencies. BH SXTs show generally no power above ~ 100 Hz and low-frequency QPOs, while the power spectra of NS SXTs extend to higher frequencies

*E-mail: farinelli@fe.infn.it

and typically show kHz QPOs (e.g. van der Klis 2000; Belloni, Psaltis & van der Klis 2002).

The X-ray outburst is accompanied by an optical outburst, with typical ratio between X-ray and optical luminosities of ~ 1000 . The reprocessing of the X-ray emission from the outer regions of the disc is a possible way to explain the ultraviolet (UV), optical and infrared (IR) emission (e.g. van Paradijs & McClintock 1995; Esin, Lasota & Hynes 2000; Coriat et al. 2009; Gandhi et al. 2011). By means of optical spectroscopy in quiescence, it has been possible to determine the mass function of several of these systems, which is the most direct way to establish if the compact accreting object is a NS or BH. Radio emission has been detected from several SXTs in outburst, and in some systems, often referred to as ‘microquasars’, jets could be resolved (Fender 2006). Simultaneous X-ray and radio observations of SXTs, albeit the global picture is not yet completely clear, seem to show some properties shared by almost all sources. In the canonical X-ray hard state, a steady and powerful jet is always observed with moderate velocity ($\Gamma \leq 2$), an associated flat radio spectrum ($\alpha \sim 0$) extending beyond the radio band and linear polarization level of a few per cent. During the source transition from hard to soft state, major radio flares are observed with ejection events stronger ($\Gamma \geq 2$) than the hard state. The radio emission gets subsequently quenched as the source has reached the soft state, and newly turns-on in the soft to hard transition at later stages of the outburst (Fender, Homan & Belloni 2009). Albeit classical studies of jets in SXTs have been performed in the radio band, in the recent years it has been shown that the contribution to the optical and IR emission can be carried out for a significant fraction by the jet, both in BH and NS X-ray binaries (Russell et al. 2006). Strong indirect evidence for optical and IR fast-variable emission from a jet has been reported by Malzac, Merloni & Fabian (2004) and Hynes et al. (2006).

In this paper we report and discuss the results of an observational campaign of XTE J1859+226 performed with *BeppoSAX* and *Rossini X-ray Timing Explorer (RXTE)* during the source 1999 outburst. In Section 2 we give an overview of the source properties from the literature. In Section 3 we report information on the periods of observations with the two satellites and on the data reduction procedure. In Section 4.2 we show the main results of the spectral analysis. In Section 5 we discuss the implications for the source accretion geometry, some considerations on the relation between the high-energy spectral features and the radio emission, the main observational difference with the systems hosting a NS and the origin of the fast temporal variability. Finally, we draw our conclusions in Section 6.

2 THE OUTBURST OF XTE J1859+226

The transient source XTE J1859+226 was first detected by the All Sky Monitor (ASM) on-board the *RXTE* satellite on 1999 October 9 (MJD 51460) at the Galactic coordinates $l = 54^\circ 05'$, $b = +8^\circ 61'$ with an intensity of 160 ± 15 mCrab in the 2–12 keV band (Wood et al. 1999). The ASM light curve (Fig. 1) shows a structure reminiscent of a fast rise and exponential decay (FRED) shape typical of SXTs, with a rise time (from 10 to 90 per cent of the peak) of about 5 d, a maximum intensity of 1.4 Crab and a decay time (e-fold) of ~ 23 d. This behaviour is however not smooth, and in the temporal interval from MJD 51468 to MJD 51479 during the decay phase, a strong flaring activity occurred.

The outburst of XTE J1859+226 was also revealed by the Burst and Transient Source Experiment (BATSE) onboard the *Compton Gamma Ray Observatory (CGRO)* up to 200 keV, with a

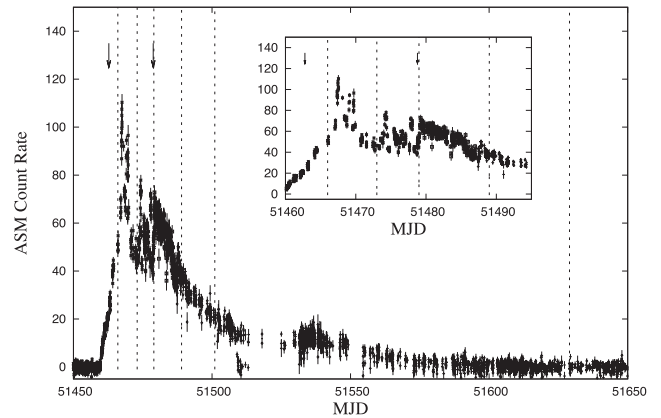


Figure 1. *RXTE*/ASM light curve of the entire XTE J1859+226 outburst and zoom of the interval MJD 51460–51495 showing the flaring activity of the source before the beginning of the e-folding decay phase. The dashed vertical lines indicate the epochs of the *BeppoSAX* observations, while the two arrows show the interval of data analysed by ST09.

peculiar behaviour: the hard X-ray flux reached its maximum (MJD 51462) while the soft X-ray flux (ASM) was still increasing (McCollough & Wilson 1999). Analysing the soft and hard X-ray temporal behaviour and comparing it with other SXTs, Brocksopp et al. (2002, hereafter B02), concluded that the hard state observed in this source at the outburst rise (despite the name of ‘soft’ X-ray transients), rather than being a peculiar behaviour of XTE J1859+226, can be a ubiquitous feature for this class of objects.

The temporal properties of the source were thoroughly investigated by Casella et al. (2004, hereafter C04) using extensive *RXTE* observations (from MJD 51462 to MJD 51546). The power spectral density (PSD) obtained with the Proportional Counter Array (PCA; 3–50 keV) showed three main types of low-frequency (1–10 Hz) QPOs, according to the centroid frequency value, the coherence parameter Q , the QPO amplitude and the shape of the underlying noise (see table 1 in C04). For C-type QPOs (the ones having $Q \gtrsim 10$), a strong anticorrelation was found between the frequency and the root mean square (rms) variability, while the rms amplitude of all the three classes increases with energy, flattening above 10 keV, ruling out a disc origin.

The source was also detected during its quiescent state in 2003 February 5 by the *Chandra X-ray Observatory*; the 0.75–2.7 keV spectrum could be fitted by a simple power law (PL) with a poorly constrained photon index $\Gamma \sim 2.4$ (Tomsick et al. 2003). The optical counterpart of XTE J1859+226 was discovered on 1999 October 12 at the position of RA(2000) = $18^{\text{h}}58^{\text{m}}41^{\text{s}}.58$, Dec.(2000) = $+22^\circ39'29''.4$, with an *R*-band magnitude of ~ 15.1 (Garnavich, Stanek & Berlind 1999) and was observed with different optical and IR telescopes, including *Hubble Space Telescope (HST)* and United Kingdom Infrared Telescope (UKIRT; Hynes et al. 2002). The optical spectrum was characterized by a strong blue continuum with weak emission lines typical of an X-ray nova in outburst (Garnavich et al. 1999; Wagner et al. 1999; Sánchez-Fernández et al. 2001; Zurita et al. 2002). Optical light curves present a FRED behaviour similar to that observed in the soft X-ray band, with maximum magnitude $V \sim 15$, quiescent magnitude $V \sim 23$, and a decay rate of 0.018 ± 0.002 mag d $^{-1}$. Evidences of three mini-outbursts near quiescence (Sánchez-Fernández et al.

Table 1. Log of *BeppoSAX* TOO observations of XTE J1859+226. For each NFI, the left column reports the time exposure (ks), the right column the mean count rate (counts s⁻¹) in the given energy band.

TOO	Epoch	MJD	LECS (0.15–4 keV)		MECS (1.5–10 keV)		HP (8–30 keV)		PDS (15–200 keV)	
1	1999 October 15	51466	Off	–	14.1	181.1 ± 0.1	14.7	63.6 ± 0.2	7.1	42.6 ± 0.1
2	1999 October 22	51473	Off	–	16.1	159.1 ± 0.1	17.2	48.8 ± 0.1	7.7	37.9 ± 0.1
3	1999 October 28	51479	0.4	163.4 ± 0.7	4.4	223.6 ± 0.2	4.0	45.8 ± 0.3	1.8	29.9 ± 0.2
4	1999 November 7	51490	0.7	139.5 ± 0.5	28.8	135.9 ± 0.1	31.4	9.6 ± 0.1	13.6	8.2 ± 0.1
5	1999 November 19	51501	4.5	73.9 ± 0.1	30.1	81.3 ± 0.1	32.3	4.3 ± 0.1	12.8	8.2 ± 0.1
6	2000 March 25	51628	18.2	0.80 ± 0.01	40.8	0.97 ± 0.01	45.2	0.97 ± 0.10	21.3	1.14 ± 0.01

2001; Zurita et al. 2002), a reflare at about 50 d after the maximum and possible superhumps (Uemura et al. 2004), were also found.

A strong radio counterpart of the source was discovered on 1999 October 11 at a flux density of ~ 10 mJy at 15 GHz with the Ryle Telescope and Very Large Array (VLA; Pooley & Hjellming 1999). The source position of RA(2000) = 18^h58^m42^s.0, Dec.(2000) = +22°39′10″.0 is consistent with the position of the optical counterpart. The radio light curve of XTE J1859+226 was characterized by five major radio flares superposed to a somewhat global fading behaviour (B02). To first approximation, the sequence of radio flares appeared to be correlated with the local minima in both the X-ray integrated rms variability and the X-ray hardness ratio at low energies (Fender et al. 2009).

The following parameters of the system were inferred from multi-wavelength observations during outburst and quiescence: orbital period of ~ 9.15 h (Garnavich & Quinn 2000; Filippenko & Chornock 2001), high inclination $i \geq 60^\circ$ (Hynes et al. 2002; Zurita et al. 2002), mass function $f(M) = 7.4 \pm 1.1 M_\odot$ (Filippenko & Chornock 2001) and source distance of ~ 6 –11 kpc (Hynes et al. 2002; Zurita et al. 2002).

The values of the orbital period and mass function were recently updated to 6.58 ± 0.05 h and $f(M) = 4.5 \pm 0.6 M_\odot$, respectively, by Corral-Santana et al. (2011), based on photometric and spectroscopic observations of the secondary star. The source distance was instead updated to $d = 4.2 \pm 0.5$ kpc by Shaposhnikov & Titarchuk (2009, hereafter ST09) using *RXTE* observations, and applying the scaling method to the Γ versus QPO or Γ versus disc normalization diagrams. With the same procedure, these authors also determined the BH mass to be $M_{\text{bh}} = 7.7 \pm 1.3 M_\odot$. Finally, the measured optical extinction $E(B - V) = 0.58 \pm 0.07$ (Hynes et al. 2002) is consistent with the average N_{H} value of $2.21 \times 10^{21} \text{ cm}^{-2}$ derived from radio maps (Dickey & Lockman 1990).

3 OBSERVATIONS AND DATA ANALYSIS

Six Target of Opportunity (TOO) observations of XTE J1859+226 were carried out from 1999 October 15 to 2000 March 27 with the *BeppoSAX*/Narrow Field Instruments (NFIs). They consist of a Low Energy Concentrator Spectrometer (LECS, 0.1–10 keV; Parmar et al. 1997), three Medium Energy Concentrator Spectrometers (MECS, 1.3–10 keV; Boella et al. 1997), a High Pressure Gas Scintillator Proportional Counter (HPGSPC, 3–120 keV; Manzo et al. 1997) and a Phoswich Detection System (PDS, 15–300 keV; Frontera et al. 1997). During the first two TOOs the LECS was switched off. The reduction of the LECS, MECS and HPGSPC data was performed with the standard *FTOOLS/SAXDAS* procedures while data from the PDS were reduced with the *XAS* package (Chiappetti & Dal Fiume 1997). The energy bands used for spectral fitting were limited to those where the response functions are well known,

i.e. 0.15–4, 1.5–10, 8–30 and 15–200 keV for the LECS, MECS, HPGSPC and PDS, respectively. In Table 1 we report the epoch of each TOO together with the exposure time of each instrument and the average count rate in the above-mentioned energy bands. A systematic error of 1 per cent was added in quadrature to the statistical uncertainties of the spectral data, on the basis of the calibration results obtained with the Crab nebula, that was observed on 1999 September 25 and on 2000 April 10, i.e. 20 d before the first TOO and 15 d after the last TOO. We used the standard response matrices officially delivered for each of the four NFIs, except for the LECS data of TOO3, TOO4 and TOO5, as when the source count rate is higher than about 50 counts s⁻¹, specific response files must be created using the *LEMAT*¹ routine.

We accumulated total energy spectra for each TOO and for each NFI. This procedure was justified by the fact that the spectral analysis showed no systematic residuals between the data and the adopted models, meaning that the time-scale of significant source spectral evolution was longer than the instrument integration time. Normalization constants, allowed to vary in the recommended ranges, were introduced to take into account known differences in the absolute cross-calibration between the detectors.²

A total of 131 *RXTE* observations from the public data archive were analysed, from 1999 October 11 (MJD 51462) to 2000 July 24 (MJD 51749). The energy spectra and PSD were extracted using the standard ‘*RXTE Cookbook*’ recipes in *HEASOFT* 6.10 analysis software release. All *RXTE* data products were corrected for PCA deadtime. The background for energy spectra was produced by *PCABACKEST* tool version 3.8. The PCA response files were created using the latest release of *PCARMF* version 11.7 and energy-to-channel conversion table version E05v04.³ The PSD was computed in the 0.01–64 Hz frequency range and normalized to give a rms deviation per Hertz. In the fitting procedure, we ignored PCA channels corresponding to energies below 3 keV and above 50 keV, while the High Energy X-ray Timing Experiment (HEXTE) spectra were constrained in 20–250 keV range. A free cross-calibration factor was used between PCA and HEXTE normalizations resulting in an expected value of ~ 0.85 for both HEXTE clusters. A systematic error of 0.5 per cent was added in the fitting process.

We also checked how many single *RXTE* pointings occurred during each *BeppoSAX* TOO and found the following results: two for TOO2 (40124-01-22-00G and 40124-01-15-00), one for TOO4 (40124-01-44-00) and three for TOO5 (40124-01-51-00, 40122-01-04-00 and 40122-01-04-01). We subsequently tried to produce strictly simultaneous *BeppoSAX* spectra in the time interval corresponding to the each single *RXTE* ID. However, because of the

¹ <http://www.asdc.asi.it/bepposax/software/saxdas/lemat.html>

² ftp://ftp.asdc.asi.it/sax/doc/software_docs/saxabc_v1.2.ps.gz

³ <http://www.universe.nasa.gov/xrays/programs/rxte/pca/doc/rmf/pcarmf-11.7>

Earth occultation time, the effective exposure time for each NFI in these subintervals was too low, and eventually it was not possible to extract spectra with a statistics good enough to perform an accurate joint *BeppoSAX*/*RXTE* analysis.

The spectral analysis was performed using the *XSPEC* package v. 12.5 (Arnaud 1996), and all the quoted errors for the spectral parameters correspond to 90 per cent confidence level for a single parameter ($\Delta\chi^2 = 2.71$). When fitting the *BeppoSAX* spectra the interstellar absorption along the source direction was modelled using the elemental abundance by Anders & Ebihara (1982) and opacities from Morrison & McCammon (1983). In contrast, because of the lack of data below 3 keV in the PCA, the spectral analysis of the *RXTE* spectra was performed by fixing the interstellar absorption to the galactic value $N_H = 0.2 \times 10^{22} \text{ cm}^{-2}$ along the source direction (Dickey & Lockman 1990).

4 RESULTS

4.1 Spectral modelling

We modelled the source X-ray spectrum with a photoelectrically absorbed two-component model, consisting of a soft and hard feature. For the soft component, we tested both a simple blackbody (BB) and the multicolour-BB model *DISKBB* in *XSPEC* (Mitsuda et al. 1984).

The latter is obtained from the convolution of several BBs at different temperatures with $T_{\text{bb}} \propto R^{-3/4}$, where R is the radial distance from the central object (Shakura & Sunyaev 1973). It is worth noting that the inner disc temperature (kT_{in}) and projected inner radius (R_{in}) of *DISKBB* have to be considered as order of magnitude, rather than exact values, because of the intrinsic simplifications of the model which do not include colour-correction factors or physical prescriptions for the inner boundary condition (e.g. Gierliński, Done & Page 2008). Despite its simplicity, the *DISKBB* model proves to be good in fitting the soft X-ray spectra of both NS and BH binary systems (McClintock & Remillard 2006; Lin, Remillard & Homan 2007).

The high-energy component of the source X-ray spectrum was instead fitted with the *BMC* model whose emerging spectral shape is given by

$$F(E) = \frac{C_n}{A+1} [S(E) + AS(E) * G(E, E_0)], \quad (1)$$

where $G(E, E_0)$ is the Green's function (GF) of the Comptonization energy operator (Titarchuk, Mastichiadis & Kylafis 1997), and $S(E)$ is the input BB spectrum. The quantity $A/(A+1)$ in equation (1) empirically describes the Comptonization fraction of the input seed photons.

The free parameters of *BMC* are the seed BB temperature kT_{bb} , the energy index α of the Comptonization GF, the Comptonization fraction $\log(A)$ and the normalization. The latter quantity is defined as $C_n = L_{39}/D_{10}^2$, where L_{39} is the seed photon source luminosity in units of $10^{39} \text{ erg s}^{-1}$, and D_{10} is the distance in units of 10 kpc, respectively.

The GF of the *BMC* model only depends on the spectral index α , namely $G(E, E_0) \propto E^{\alpha+3}$ for $E < E_0$, and $G(E, E_0) \propto E^{-\alpha}$ for $E > E_0$. As the GF is a broken PL with no cut-off, the output spectrum at high energies is yet a PL. When the data show the presence of a high-energy rollover, this must be taken into account by multiplying *BMC* by an e-folding factor $\propto e^{-E/E_f}$ (*HIGHECUT*).

In this sense, *BMC* is the most general available Comptonization model: it just measures the relative contribution of the direct and

Comptonized component and the slope of the Comptonization spectrum, no matter which is the underlying physical process and thus having no limitation in its applicability. The origin of the observed features is demanded in a second step to a scientific discussion.

4.2 *BeppoSAX* and *RXTE* spectra

The spectral analysis was first carried out with *BeppoSAX*, because of its broader energy band (0.1–200 keV) with respect to *RXTE* (3–200 keV), particularly in the critical region where interstellar absorption is present.

The *BeppoSAX* spectra of the source show the presence of a thermal component at low energies (Fig. 2). However a simple blackbody (BB) model does not provide in general acceptable fits, while the *DISKBB* better describes the data. Thus we adopted *WABS**(*DBB*+*BMC*) as basic spectral model for the continuum emission.

During TOO1, the presence of a high-energy cut-off in the spectrum was clearly evident. Indeed, the basic model does not provide acceptable fit ($\chi^2/\text{dof} = 690/110$), while multiplying *BMC* by an e-folding factor, the model *WABS**(*DBB*+*BMC***HIGHECUT*) gives a satisfactory result ($\chi^2/\text{dof} = 131/109$).

During TOO2, the spectral properties of the source were very similar to TOO1 (Fig. 3). In particular, the model *WABS**(*DBB*+*BMC*) without cut-off gives $\chi^2/\text{dof} = 451/160$, while with cut-off we find $\chi^2/\text{dof} = 99/105$.

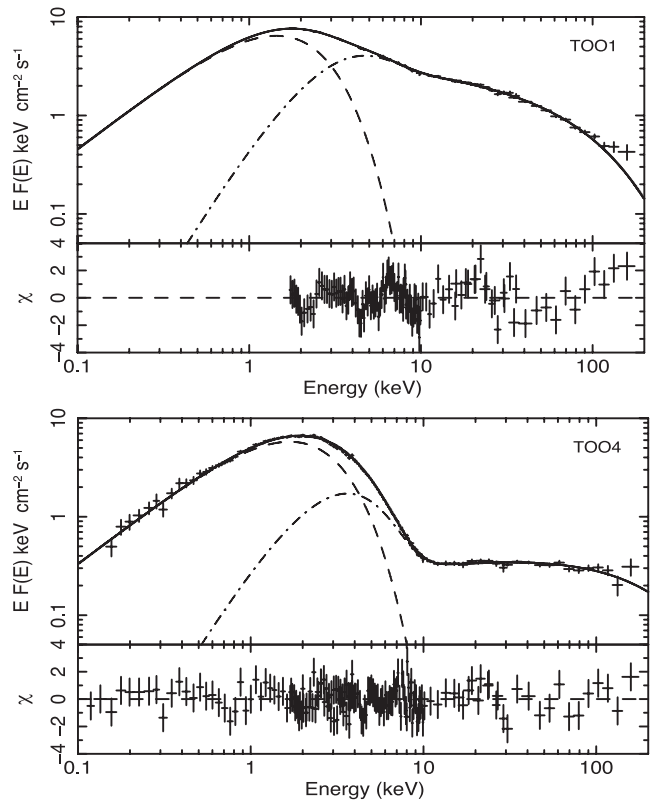


Figure 2. Absorption-corrected deconvolved spectra in $EF(E)$ units, best-fitting model *DISKBB*+*BMC* and residuals between the data and the model in units of σ for *BeppoSAX* TOO1 and TOO4 of XTE J1859+226. The single spectral components are also plotted: *DBB* (dashed line) and *BMC* (dotted-dashed line). The emission line, marginally evident in the first and second *BeppoSAX* TOO, has not been included here.

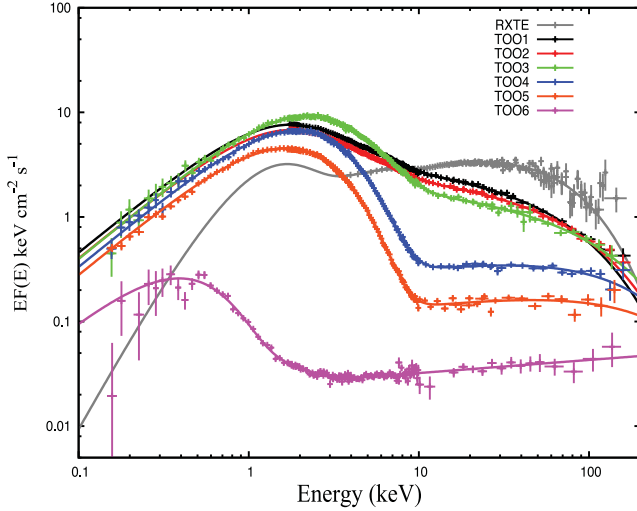


Figure 3. Spectral evolution of XTE J1859+226 across the whole outburst. The spectra of the six *BeppoSAX* TOOs and that corresponding to the first *RXTE* observation (MJD 51462) are reported.

The spectrum of the source during TOO3 at higher energies was slightly harder than that of TOO1 and TOO2. In particular, the model $\text{WABS}^*(\text{DBB}+\text{BMC})$ provides $\chi^2/\text{dof} = 167/158$, while $\text{WABS}^*(\text{DBB}+\text{BMC}^*\text{HIGHECUT})$ gives $\chi^2/\text{dof} = 133/158$. The probability of chance improvement (PCI) for the inclusion of the cut-off components is ~ 0.08 , and it was obtained through the F -test routine for discriminating among two different spectral models for the case of multiplicative component (Press et al. 1992).

During TOO4, the presence of the high-energy cut-off also proved to be marginal (Figs 2 and 3). The models $\text{WABS}^*(\text{DBB}+\text{BMC})$ and $\text{WABS}^*(\text{DBB}+\text{BMC}^*\text{HIGHECUT})$ indeed give $\chi^2/\text{dof} = 166/152$ and $135/151$, respectively, with $\text{PCI} = 0.2$ in both cases.

The gradual shift towards higher energies of the spectral cut-off became evident at the time of TOO5, with the model $\text{WABS}^*(\text{DBB}+\text{BMC})$ yielding $\chi^2/\text{dof} = 164/147$, and model $\text{WABS}^*(\text{DBB}+\text{BMC}^*\text{HIGHECUT})$ yielding $\chi^2/\text{dof} = 160/146$. Actually, it was only possible to put a lower limit on $E_f \gtrsim 130$ keV.

At the time of the last *BeppoSAX* observation, TOO6, the source was moving towards quiescence with a significant drop in the bolometric luminosity. At low energies, the statistics of the source was significantly worse with respect to the previous observations (Fig. 3). At high energies, the spectrum was dominated by a pure PL component and, unlike the case of TOO4 and TOO5, we could not put even a lower limit on the value of the cut-off energy E_f . Thus, we just used the model $\text{WABS}^*(\text{DBB}+\text{BMC})$ which yields $\chi^2/\text{dof} = 162/133$.

During the first two TOOs, we found some evidence for the marginal presence of a Fe emission line (see Fig. 2). Modelling the feature with a Gaussian component added to the continuum, the fit improves to $\chi^2/\text{dof} = 111/107$ and $85/103$ for TOO1 and TOO2, respectively. In both cases, the line width σ was fixed to 0.2 keV, as leaving it free during the fitting procedure, the centroid of the line shifts towards too low values ($E_c \sim 6$ keV). Having in mind the issues reported by Protassov et al. (2002) about the use of F -test in the case of emission lines, we empirically tested the significance of the feature. Specifically, we generated 10^4 fake spectra for all the NFIs using for the continuum the best-fitting model $\text{WABS}(\text{DISKBB}+\text{BMC}^*\text{HIGHECUT})$ without the Gaussian emission line, and with the same time exposure of the true spectra for each NFI.

We then fitted the simulated spectra first with the continuum model alone, and later with inclusion of the line (with $\sigma = 0.2$ keV). For each simulated spectrum, we computed the value $F_{12} = (\chi_1^2 - \chi_2^2)/(\nu_1 - \nu_2)\nu_2/\chi_2^2$, where F_{12} is the probability distribution function (Bevington & Robinson 2003). Then, we computed the number of spectra N satisfying $F_{12} > F_{12}^{\text{obs}}$, where F_{12}^{obs} was computed on the true data. We found that the fraction of simulated spectra obeying the above condition is 38×10^{-4} for TOO1 and 140×10^{-4} for TOO2, respectively.

These values represent the empirically estimated PCI for the addition of the emission line.

As far as the *RXTE* spectra are concerned, we note that ST09 considered only the PCA data in their spectral analysis of the early part of the outburst of XTE J1859+226. The lack of spectral coverage below 3 keV and the lower energy resolution of the PCA with respect to the LECS and MECS experiments onboard *BeppoSAX*, allowed ST09 to fit the source spectrum with a simple photoelectrically absorbed GAUSSIAN+BMC model. However, the *BeppoSAX* low-energy data clearly showed the presence of a soft thermal component, which actually carries out a significant part of the source luminosity (see Table 2). Thus, driven by the *BeppoSAX* results, we tested both $\text{WABS}^*(\text{BB}+\text{BMC})$ and $\text{WABS}^*(\text{DISKBB}+\text{BMC})$ models also on the *RXTE* spectra. We found that in both cases, they satisfactorily fit the data, strongly reducing the significance of the Gaussian component. For consistency with the *BeppoSAX* results, we thus have chosen as reference model $\text{WABS}^*(\text{DISKBB}+\text{BMC})$, fixing the photoelectric absorption to the value across the source direction $N_H = 0.2 \times 10^{22} \text{ cm}^{-2}$. However, given that more than one hundreds *RXTE* observations were performed during the source outburst, instead of reporting all the best-fitting parameters in a table, we decided to plot them as a function of the MJD overplotted with the *BeppoSAX* results (Fig. 4).

5 DISCUSSION

5.1 Spectral evolution across the outburst

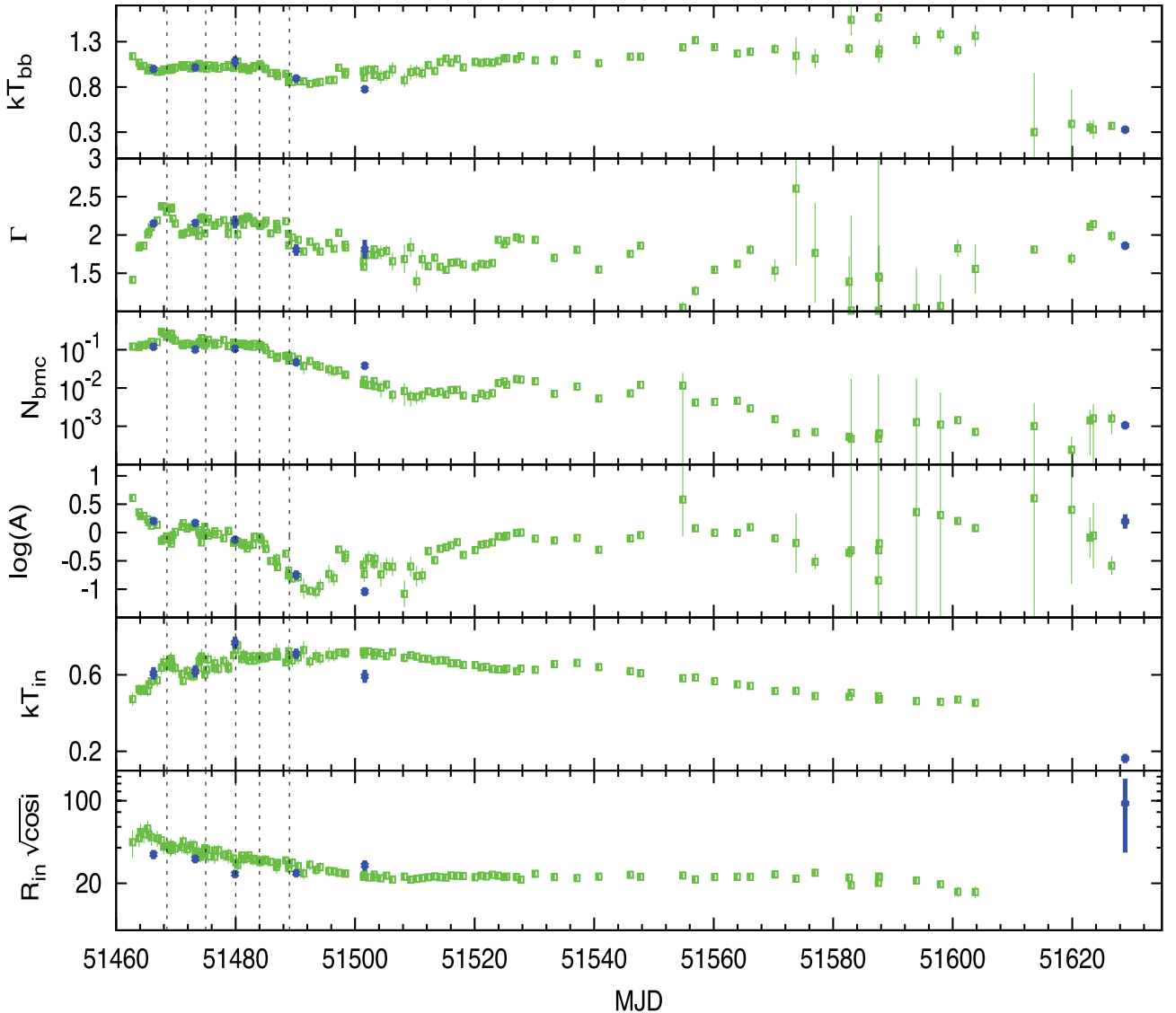
The extended temporal coverage of XTE J1859+226 by *RXTE* together with the *BeppoSAX* observations allowed us to deeply investigate the spectral evolution of the source during the whole outburst (Fig. 3).

The X-ray continuum is characterized by the presence of a soft thermal component, described by a multicolour-BB model (DISKBB) and, at higher energies, by the convolution of a seed BB spectrum with a Compton up-scattering GF (BMC). Even if the data did not allow to fix equal BB and DISKBB temperatures (kT_{bb} and kT_{in} , respectively) in the fit, we interpret them as having a common origin in the accretion disc. In particular, as $kT_{\text{bb}} > kT_{\text{in}}$, it is worth attributing the BB temperature to the innermost part of the accretion disc. We refer to this region, where the gas gets hotter and most of Comptonization takes places, as the transition layer or Compton cloud (Titarchuk & Fiorito 2004). A similar spectral modelling using BMC was also adopted by Montanari, Titarchuk & Frontera (2009, hereafter M09) in their *BeppoSAX* analysis of XTE J1650–500, even if in that case a simple BB could adequately fit the soft excess.

In Fig. 4 we report the behaviour of the spectral parameters of the best-fitting model $\text{WABS}^*(\text{DBB}+\text{BMC}^*\text{HIGHECUT})$ as a function of time (MJD), while in Fig. 5 we show the integrated (0.1–64 Hz) rms and the soft (2–20 keV) and hard (20–200 keV) deconvolved X-ray fluxes obtained in the period where also radio observations were available (see Section 5.3).

Table 2. Best-fitting parameters of the model $\text{WABS}^*(\text{DBB}+\text{BMC}^*\text{HIGHECUT})$ for the six *BeppoSAX* observations of XTE J1859+226. The projected inner disc radius and luminosity are computed assuming a distance of 4.2 kpc.

Parameter	TOO1	TOO2	TOO3	TOO4	TOO5	TOO6
$N_{\text{H}} (\times 10^{22} \text{ cm}^{-2})$	$0.31^{+0.13}_{-0.13}$	$0.32^{+0.13}_{-0.13}$	$0.28^{+0.01}_{-0.01}$	$0.30^{+0.01}_{-0.01}$	$0.27^{+0.01}_{-0.01}$	$0.39^{+0.09}_{-0.08}$
$kT_{\text{in}} (\text{keV})$	$0.61^{+0.03}_{-0.03}$	$0.62^{+0.03}_{-0.03}$	$0.77^{+0.03}_{-0.03}$	$0.71^{+0.03}_{-0.03}$	$0.59^{+0.03}_{-0.03}$	$0.16^{+0.03}_{-0.02}$
$R_{\text{in}} \sqrt{\cos i} (\text{km})$	35^{+3}_{-3}	32^{+3}_{-3}	24^{+2}_{-2}	24^{+2}_{-2}	28^{+3}_{-3}	95^{+84}_{-33}
$kT_{\text{bb}} (\text{keV})$	$1.00^{+0.04}_{-0.04}$	$1.01^{+0.04}_{-0.04}$	$1.08^{+0.06}_{-0.05}$	$0.89^{+0.04}_{-0.03}$	$0.77^{+0.04}_{-0.03}$	$0.32^{+0.04}_{-0.04}$
Γ	$2.15^{+0.04}_{-0.04}$	$2.15^{+0.04}_{-0.04}$	$2.17^{+0.08}_{-0.09}$	$1.80^{+0.07}_{-0.08}$	$1.81^{+0.12}_{-0.13}$	$1.87^{+0.05}_{-0.05}$
$\log(A)$	$0.20^{+0.04}_{-0.03}$	$0.17^{+0.04}_{-0.03}$	$-0.13^{+0.06}_{-0.05}$	$-0.75^{+0.09}_{-0.07}$	$-1.04^{+0.09}_{-0.06}$	$0.19^{+0.14}_{-0.13}$
N_{bmc}	$0.120^{+0.004}_{-0.004}$	$0.10^{+0.004}_{-0.004}$	$0.11^{+0.01}_{-0.01}$	$0.047^{+0.008}_{-0.008}$	$0.038^{+0.007}_{-0.008}$	$1.06^{+0.16}_{-0.11} \times 10^{-3}$
$E_{\text{f}} (\text{keV})$	77^{+7}_{-6}	94^{+11}_{-9}	130^{+57}_{-32}	159^{+72}_{-39}	> 130	—
$F_{\text{disc}}/F_{\text{tot}}$	0.56	0.56	0.64	0.77	0.75	0.67
$F_{0.1-200 \text{ keV}}^a$	3.67	3.23	3.76	2.37	1.59	0.10
$L_{0.1-200 \text{ keV}}^b$	7.81	6.90	8.02	5.05	3.40	0.21
χ^2/dof	131/109	99/105	133/158	134/150	160/146	162/138

^aIn units of $10^{-8} \text{ erg cm}^{-2} \text{ s}^{-1}$.^bIn units of $10^{37} \text{ erg s}^{-1}$.**Figure 4.** Evolution of the parameters of the BMC and DISKBB components over the outburst of XTE J1859+226 for the *RXTE* (green points) and *BeppoSAX* (blue points) observations. The vertical dashed lines indicate the times of the five radio flares identified by B02 (see also Fig. 5).

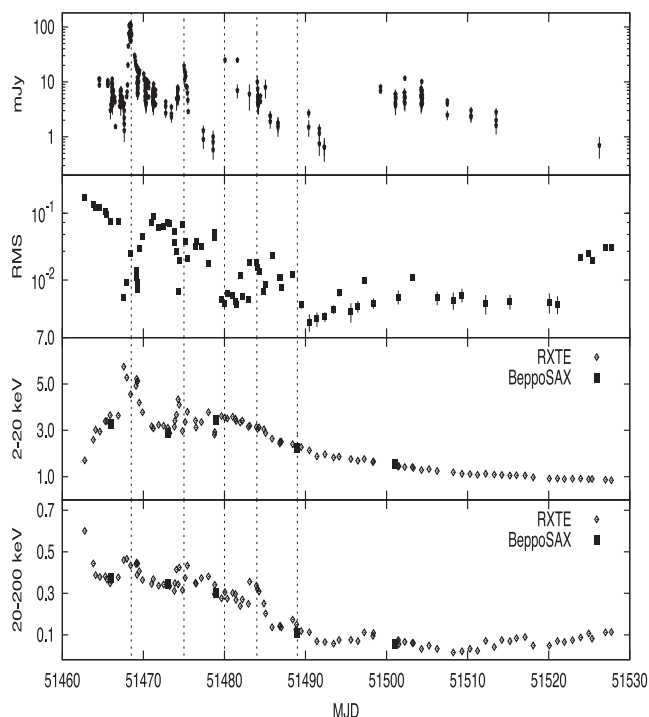


Figure 5. From top to bottom: radio light curve at different wavelengths (see Section 5.3), integrated 0.1–64 Hz rms, 2–20 and 20–200 keV fluxes in units of 10^{-9} erg cm $^{-2}$ s $^{-1}$ obtained from the deconvolved best-fitting model DISKBB+BMC using both *BeppoSAX* and *RXTE*. The time period of the plotted data corresponds to that of the available radio observations.

As already reported by B02, XTE J1859+226 entered its outburst in a hard state, with the peak of the soft X-ray light curve delayed by a few days (Fig. 5, see also fig. 1 in B02). At the peak of the hard X-ray luminosity (MJD 51462) the source spectrum was characterized by a dominating thermal Comptonization (TC) feature, with cut-off energy below 100 keV (Fig. 3) and photon index $\Gamma \sim 1.5$. In this phase the disc contribution to the total luminosity was less than 20 per cent, and the PSD showed high temporal variability (rms ~ 30 per cent, see Fig. 5), both features typical of a canonical hard state (Remillard & McClintock 2006).

During the rising phase of the soft X-ray flux (Fig. 1), the Comptonization spectral index Γ progressively increased, reaching its maximum (~ 2.5) in coincidence with the soft X-ray peak. In the same period, the Comptonization fraction $\log(A)$ decreased, as well as the BMC seed photon temperature. On the other hand an increase of the inner disc temperature kT_{in} occurred, together with a decrease of the projected inner disc radius. The simultaneous and monotonic decrease of the rms is also indicative of a spectral transition from hard to soft state.

This trend of the spectral parameters is usually expected in the scenario of the truncated disc model (Done, Gierliński & Kubota 2007).

The subsequently observed flaring phase of the ASM light curve is claimed to mainly originate in the accretion disc, which dominates the spectral emission below 10 keV (Fig. 2). Indeed between MJD 51466 and MJD 51480, fluctuations in the inner disc temperature (however not in its normalization) occur, and they are approximately coincident with the secondary peaks of the ASM light curve.

Not surprisingly, any variation of the disc properties is expected to have physical consequences in the radiative processes of the

Comptonization region: hardening and softening of the high-energy X-ray spectrum are visible in Fig. 4 through fluctuations of Γ . Once again, changes of the geometrical extension of the corona, in response to this effect, are still visible looking at the behaviour of $\log(A)$. Yet, during the flaring phase, significantly less visible changes are observed in the kT_{bb} value or BMC normalization.

It is of particular interest the source behaviour in the period between *BeppoSAX* TOO4 (MJD 51490) and TOO5 (MJD 51501), during the smooth ASM exponential decay phase. In this phase, the disc contributed more than 70 per cent to the total luminosity (see Figs 2 and 3), and, at the same time, rms was $\lesssim 5$ per cent, typical of a soft state.

However, the photon index was $\Gamma \sim 1.8$, which is actually a value closer to a hard state (see e.g. XTE J1650–500 in M09).

Note also that this time period also corresponds to the minimum value achieved by the Comptonization fraction parameter $\log(A)$, as shown in Fig. 4, thus presumably in this phase the Compton cloud reaches its minimum size. As also shown by the BATSE light curve reported in B02 and by *BeppoSAX* and *RXTE* in Fig. 5, while moving towards quiescence XTE J1859+226 experienced an increase of the hard X-ray flux (> 20 keV) around MJD 51520, with a corresponding increase of the rms (~ 10 per cent).

This feature however does not necessarily imply a temporary soft to hard transition at all. Actually, Fig. 4 shows that the rise of the hard X-ray luminosity was accompanied by an increase of the Comptonization fraction $\log(A)$ and a steepening of the photon index Γ . At high energies, the spectrum thus became slightly softer but globally brighter. This trend appears puzzling when looking at the behaviour of the two soft seed photon components. Indeed, a slight increase of the disc temperature kT_{in} occurred a few days later (around MJD 51530) after the new rise of the hard X-ray luminosity, and appears not tightly correlated with changes in the BMC parameters $\log(A)$ and Γ .

The only appreciable correlated variation is found in the BMC normalization (but not in kT_{bb}), which actually also increased around MJD 51520 more or less tracing the behaviour of Γ . Thus, we interpret the rebrightening of the hard X-ray luminosity as an enhancement of the amount of photon supply from the innermost region (BMC normalization) such that this effect compensated, in terms of Comptonization energy flux, the steepening of the photon index Γ .

Note that this is a different behaviour with respect to what happened at the beginning of the outburst, where the coronal behaviour appeared mostly dictated by changes in the DISKBB component (see above).

The increased time intervals between each *RXTE* pointing for MJD $\gtrsim 51540$ and the reduced statistical quality of the high-energy *RXTE* spectra did not allow a thorough mapping of the evolution of the source spectral parameters.

However, more than 5 months after the outburst onset (MJD 51629), *BeppoSAX* observed the source when the 0.1–200 keV flux was $\sim 10^{-9}$ erg cm $^{-2}$ s $^{-1}$. The broad-band coverage and sensitivity of *BeppoSAX* allowed the unique opportunity to catch the source close to quiescence with an excellent data quality (Fig. 3). In the phase down to quiescence, the spectrum of XTE J1859+226 is characterized by a strong PL component with $\Gamma \sim 1.9$ and no evidence of cut-off. The accretion disc contributes yet to a significant fraction of the total luminosity (about 67 per cent), but now is much cooler ($kT_{\text{bb}} \sim 0.3$ keV, $kT_{\text{in}} \sim 0.2$ keV), and the Comptonization fraction is at the same level of the rising phase of the outburst.

The very low temperature of the direct disc component does not allow its detection by the PCA, and this explains the gap of data

points in the two lower panels of Fig. 4. The spectral shape of the last *BeppoSAX* observation can be interpreted as a new significant increase of the Compton cloud characteristic size, together with a very high electron temperature, consequences of a strongly reduced efficiency in Compton cooling by the seed photons.

5.2 Justification of the adopted spectral model for describing the high-energy emission

The high-energy emission of BH sources in different spectral states has been fitted with several *XSPEC* Comptonization models such as *COMPTT* (Cadolle Bel et al. 2006), *COMPPS* (Frontera et al. 2001) or *EQPAIR* (Del Santo et al. 2008). All the above-mentioned models contain a detailed treatment of the radiative transfer physics, but each of them presents its own drawbacks.

In particular, it is worth emphasizing that both *COMPTT* (Titarchuk 1994) and *COMPPS* (Poutanen & Svensson 1996) are *static thermal Comptonization models* with different ranges of applicability for the plasma electron temperature and optical depth (preferably low kT_e and high τ for *COMPTT* and the opposite for *COMPPS*). On the other hand *EQPAIR* (Coppi 1999) allows to compute Comptonization spectra for a plasma which can be purely thermal or hybrid (thermal plus non-thermal electron distribution).

Thus, when one of such models is used to fit the source spectra at high energies, it is implicitly assumed that the spectral changes occur in the framework of static-only TC processes (*COMPTT*, *COMPPS*) or due to a switch from static thermal to hybrid Comptonization (*EQPAIR*).

By fitting the *RXTE* spectrum of XTE J1859+226 during the bright hard state at the beginning of the outburst (MJD 51462, see Fig. 3) with *DISKBB*+*COMPPS* model, assuming spherical geometry of the Compton cloud, we found $kT_e \sim 30$ keV and $\tau \sim 1$ (with Comptonization parameter $Y \approx 0.2$). Following the source evolution from the hard to the soft state we note however that e.g. the fit of the *BeppoSAX* spectra provided an electron temperature kT_e increasing from ~ 50 (TOO1) to ~ 200 keV (TOO5) with a corresponding decrease of the optical depth from $\tau \sim 1$ to ~ 0.2 , respectively, and $Y \approx 0.3$ – 0.4 .

The χ^2 values were acceptable in all cases, but in our opinion it is difficult to explain such a behaviour during a hard to soft transition. In particular, the enhanced disc contribution to the total luminosity (see Table 2) is expected to provide strong Compton cooling of the coronal electrons and their temperature should decrease rather than increase.

It is also worth mentioning that because of the *RXTE* and *BeppoSAX* high-energy threshold around 200 keV it was not possible to find evidence of any additional PL-like component above the energy rollover such as reported e.g. in GX 339-4 by Del Santo et al. (2008) with the spectrometer on *INTEGRAL* (SPI). Thus, hybrid Comptonization (*EQPAIR*), rather than excluded, is not required by the data. The progressive increase of the high-energy cut-off during the hard to soft transition, together with the spectral index steepening, can be more easily explained by the transition from a TC to bulk Comptonization (BC) dominated state (e.g. M09).

Unfortunately, specific models for BC in BH sources are not yet available. The *COMPTB* model of Farinelli et al. (2008) is based on an assumption of subrelativistic bulk motion, expected to hold in NS systems due to strong radiation pressure from the NS surface, but not in BHs.

Actually, our choice of BMC was mostly motivated by the fact that with its parametrization, it represents the best compromise between a phenomenological and physical description of the high-energy

source spectral behaviour, possibly avoiding contradictory results which may be obtained, e.g. using static TC models.

5.3 Correlation between X-ray and radio emission

A thorough study of the correlation between the X-ray and radio emission of XTE J1859+226 was previously carried out by B02. In Fig. 5 we report the cumulative light curve of the source obtained from several observing facilities at frequencies ranging from 1.22 to 22.5 GHz in the period from 1999 October 13 (MJD 51464) to 1999 December 13 (MJD 51525), and we address the reader to B02 for details.

The radio light curve shows a rather complex behaviour, with fluxes ranging from 0.5 to 100 mJy, and five major flares identified by B02 (drawn as vertical lines in Figs 4 and 5) occurring over an otherwise globally fading behaviour.

Starting from the results of the X-ray spectral analysis, we searched for correlated patterns between the radio emission and the source spectral parameters in spite of integrated X-ray fluxes.

To avoid biases in the obtained results, due to different observing times at different frequencies, we preliminary normalized the radio fluxes to those at 15 GHz, using the relation $F(15 \text{ GHz}) = F(\nu)(15 \text{ GHz}/\nu)^\alpha$ mJy, with the spectral index α reported in table 1 of B02. We then considered the normalized radio light curve and single parameters of the *DISKBB*+*BMC* model averaged over half and one day, respectively, and we calculated the Spearman correlation coefficient r . Because the number of points was more than 20, we also calculated the significance of the correlation using the associated t variable of the Student's distribution.

The strongest X–radio correlation (>99 per cent confidence level) is found, over 1-d time-scale, between the radio flux and both the spectral photon index Γ and BMC normalization (N_{bmc}), with $r \sim 0.6$ in both cases (Fig. 6).

On the other hand, the hard X-ray flux (given by the convolution term in equation 1) is proportional to N_{bmc} , thus in turn its positive correlation with the radio emission is eventually expected as well. We find indeed that it is similar to that observed with the aim of BATSE data (see fig. 8 in B02).

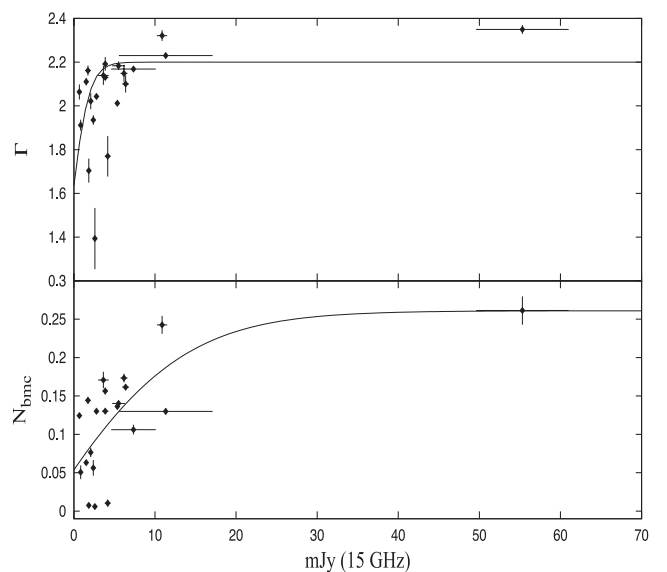


Figure 6. Spectral photon index Γ (upper panel) and BMC normalization (lower panel) as a function of the radio flux normalized at 15 GHz for XTE J1859+226. Data have been averaged over 1 d.

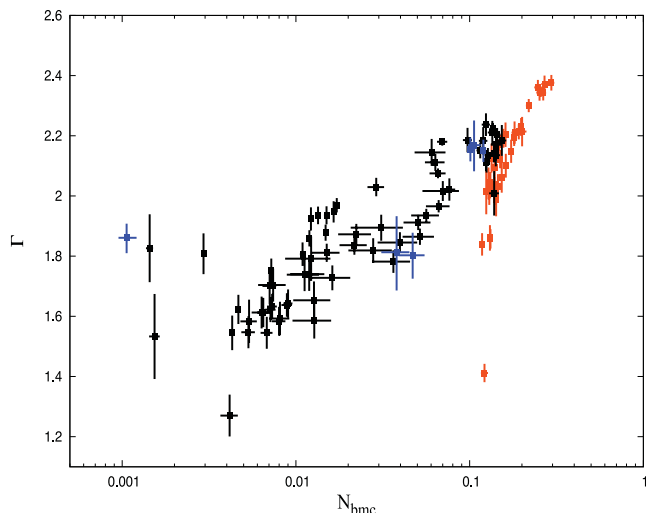


Figure 7. Spectral photon index Γ versus BMC normalization for the *RXTE* data set analysed by ST09 (orange), plus the second part of the outburst (black) and the six *BeppoSAX* TOOs (blue). For clarity purposes we plotted only the points for which the ratio between the best-fitting value and the 1σ error determined by *XSPEC* is $\gtrsim 3$.

It is interesting to observe that brighter and steeper X-ray spectra are associated with brighter radio events, with a possible *saturation effect* of the photon index Γ for increasing radio fluxes.

As reported in Fig. 7, the same saturation effect is instead not observed in a diagram of Γ versus N_{bmc} , a typical feature of most, albeit not all, black hole candidates (BHCs; ST09).

The index saturation in a Γ versus N_{bmc} or Γ versus ν_{QPO} diagram is interpreted as an indirect evidence for the presence of a converging flow (bulk motion) close to the central object in BH sources, and it is expected to occur when the optical depth $\tau \gg 1$ (Laurent & Titarchuk 2007; Titarchuk & Seifina 2009).

The thorough monitoring with *RXTE* during the whole outburst of XTE J1859+226 (Fig. 4) seems to exclude the possibility of an incomplete sampling problem.

As $\tau \propto \dot{M}$, one possibility, albeit speculative, is that in this source the accretion rate \dot{M} does not exceeds the critical value above which the Comptonization parameter Y , and in turn the spectral index Γ , becomes insensitive to τ .

The apparent index saturation in the Γ versus radio diagram is thus challenging in this context.

Correlation patterns between the radio emission and the integrated rms variability were investigated by Fender et al. (2009) who found that the five radio flares identified by B02 occurred around periods of reduced rms. This is almost evident looking at Fig. 5, albeit the correlation is much less significant ($r \lesssim 0.2$). Also, the different behaviour of GX 339–4 and possibly XTE J1550–564 seems to point against a direct casual link.

5.4 Transition layer as a formation site for the fast X-ray variability

One of the most established observational results of BH systems is that their PSD strongly correlates with the source spectral state. During the hard state, the rms variability is high (up to 40 per cent) and the PSD is described by a broken PL with a flat plateau up to the break frequency. When the source moves progressively towards the intermediate and soft state, the rms variability decreases below 10 per cent and the PSD is a PL with index 1.0–1.5 (Remillard & Mc-

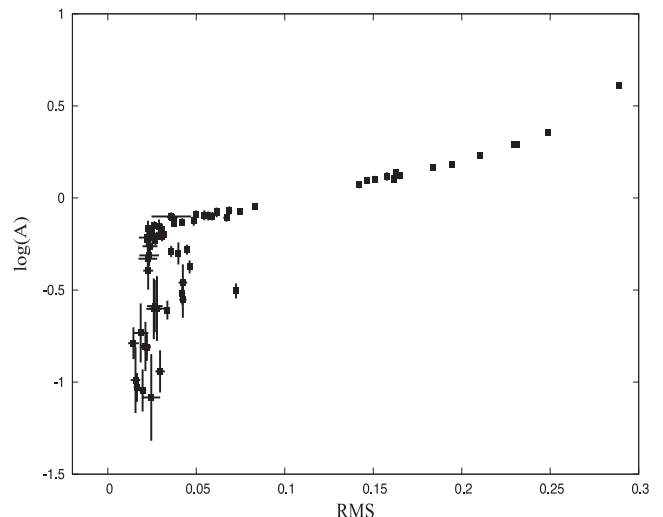


Figure 8. Fraction of Comptonized seed photons, parametrized through $\log(A)$ in BMC, versus integrated 0.1–64 Hz rms variability using *RXTE* data.

Clintock 2006). The rapid variability down to $\sim 10^{-2}$ s is probably mostly dictated by variations of the Comptonization region (TL), as the characteristic viscous time-scale of the accretion disc is several hundreds of seconds (Churazov, Gilfanov & Revnivtsev 2001).

Models for explaining the rapid variability as a function of the source spectral state have been proposed, e.g. by Titarchuk, Shaposhnikov & Arefiev (2007) and Ingram & Done (2011) in the framework of propagating perturbations in bounded configurations.

In order to strengthen the hypothesis that rapid variability originates in the TL, in Fig. 8 we present a plot of the $\log(A)$ parameter of BMC versus the integrated 0.1–64 Hz rms of XTE J1859+226. A tight positive correlation is observed between the two quantities for rms $\gtrsim 5$ per cent. The Spearman rank correlation coefficient in this case is $r = 0.95$, while including the whole data it is $r = 0.83$. As it can be seen from the definition of the BMC model (equation 1), $\log(A)$ quantifies the contribution of the Comptonized spectrum with respect to the input seed photon population. To first approximation, $\log(A)$ is an indirect measurement of the size of the Compton cloud. The fact that when $\log(A)$ increases, the corresponding source rms increases as well, is thus a strong additional probe that it is the Compton cloud the site of origin of the rapid variability.

On the other hand, unlike the case of the broad-band noise component, the origin of low-frequency QPOs both in NS (10–60 Hz) and BH (0.1–10 Hz) sources is still controversial, as either models proposing a Lense–Thirring disc precession origin (e.g. Stella & Vietri 1998; Stella, Vietri & Morsink 1999; Schnittman 2005; Schnittman, Homan & Miller 2006) or magnetoacoustic oscillations of the Comptonization region (e.g. Titarchuk & Osherovich 1999; Wagoner, Silbergleit & Ortega-Rodríguez 2001) have proved to be in good agreement with observations.

A tight correlation between the spectral photon index Γ of the Compton cloud and characteristic C-type QPOs, which have variable frequency (0.1–10 Hz) and high coherence parameter ($Q \gtrsim 10$), has been observed in a large sample of BH sources by ST09. Additionally, C04 (see their fig. 3) found a tight anticorrelation between the rms and ν_{QPO} for QPOs of the same type. These observational features, together with the fact that usually QPOs show greater amplitude at higher energies, apparently would favour the Compton cloud, rather than the accretion disc, as the region where QPOs form.

However, it is worth noting that the above-mentioned correlations are not in contradiction with a tilted disc origin, if most of the disc thermal soft radiation is intercepted and Comptonized by the hotter inner region. This interaction indeed, would shift to higher energy the soft photons modulated at the Lense–Thirring disc precessional frequency, at the same time preserving the Γ versus ν_{QPO} and rms versus ν_{QPO} relations.

It is also worth mentioning that no correlation with the rms was observed by C04 for A-type and B-type QPOs ($7 \lesssim \nu \lesssim 8$ Hz, $Q \lesssim 3$ and $4.5 \lesssim \nu \lesssim 6.5$ Hz, $Q \gtrsim 6$, respectively) and that the Γ versus QPO correlations diagrams for BH mass determination with the scaling method were produced by ST09 using only C-type QPOs.

This pattern behaviour could be indicative of a different physical origin for the various types of QPOs with C-type ones associated with magnetoacoustic oscillations of the TL (Titarchuk & Fiorito 2004) and A-type and B-type ones originating either in a formation site away from the TL or in some physical process (e.g. jet/corona connection) almost independent on the geometrical variations of the TL itself.

6 CONCLUSIONS

The joint *BeppoSAX/RXTE* analysis that we performed of the X-ray nova XTE J1859+226 during its 1999 outburst has demonstrated the importance of getting simultaneous spectral and temporal information during the source evolution. The extensive observational campaign performed by the two satellites indeed allowed us to map thoroughly XTE J1859+226 from the onset of its outburst down a phase close to quiescence. We modelled the hard X-ray component with the BMC model which has the advantage of being a fully generic Comptonization model, suitable to be applied in any physical regime because the shape of the up-scattering GF in BMC can be considered as general as possible.

The source experienced all the canonical spectral states of BHCs from hard to soft (Fig. 3). During the soft state, with a disc contribution to the total luminosity higher than 70 per cent and an rms < 10 per cent, the high-energy spectral index, with $\Gamma \sim 1.8$, was actually closer to typical values of the hard state.

A significant correlation was observed between Γ and the radio emission, with a possible effect of index saturation at the brightest radio emission levels. Additionally, we found a tight correlation between the Comptonization fraction of the seed photons, parametrized through $\log(A)$, and the source rms, which allowed us to strengthen the claim that most of the source variability originates in the transition layer, where also Comptonization is the dominating process. This correlation is new and can be of key interest in understanding the accretion geometry of X-ray binary systems hosting either a BH or a NS.

We thus strongly suggest to test it on a large sample of sources, which is possible due to the large amount of archival *RXTE* data.

ACKNOWLEDGMENTS

RF is grateful to Lev Titarchuk for useful discussions related to the spectral evolution of X-ray novae, and acknowledges financial support from agreement ASI-INAF I/009/10/0. The authors also acknowledge the anonymous referee whose detailed report was helpful in better outlining the most important results of the paper.

REFERENCES

- Anders E., Ebihara M., 1982, *Geochim. Cosmochim. Acta*, 46, 2363
- Arnaud K. A., 1996, in Jacoby G. H., Barnes J., eds, *ASP Conf. Ser. Vol. 101, Astronomical Data Analysis Software and Systems V*. Astron. Soc. Pac., San Francisco, p. 17
- Belloni T., Psaltis D., van der Klis M., 2002, *ApJ*, 572, 392
- Bevington P. R., Robinson D. K., 2003, *Data Reduction and Error Analysis for the Physical Sciences*. McGraw-Hill, New York, p. 204
- Boella G. et al., 1997, *A&AS*, 122, 327
- Brockspoll C. et al., 2002, *MNRAS*, 331, 765 (B02)
- Cadotte Bel M. et al., 2006, *A&A*, 446, 591
- Casella P., Belloni T., Homan J., Stella L., 2004, *A&A*, 426, 587 (C04)
- Cherepashchuk A. M., 2000, *Space Sci. Rev.*, 93, 473
- Chiappetti L., Dal Fiume D., 1997, in Di Gesu V., Duff M. J. B., Heck A., Maccarone M. C., Scarsi L., Zimmerman H. U., eds, *Proc. Fifth Workshop, Data Analysis in Astronomy*. World Scientific Press, Singapore, p. 101
- Churazov E., Gilfanov M., Revnivtsev M., 2001, *MNRAS*, 321, 759
- Coppi P. S., 1999, in Poutanen J., Svensson R., eds, *ASP Conf. Ser. Vol. 161, High Energy Processes in Accreting Black Holes*. Astron. Soc. Pac., San Francisco, p. 375
- Coriat M., Corbel S., Buxton M. M., Bailyn C. D., Tomsick J. A., Kording E., Kalemci E., 2009, *MNRAS*, 400, 123
- Corral-Santana J. M., Casares J., Shahbaz T., Zurita C., Martínez-Pais I. G., Rodríguez-Gil P., 2011, *MNRAS*, 413, L15
- Del Santo M., Malzac J., Jourdain E., Belloni T., Ubertini P., 2008, *MNRAS*, 390, 227
- Dickey J. M., Lockman F. J., 1990, *ARA&A*, 28, 215
- Done C., Gierliński M., Kubota A., 2007, *A&AR*, 15, 1
- Esin A. A., Lasota J.-P., Hynes R. I., 2000, *A&A*, 354, 987
- Farinelli R., Titarchuk L., Paizis A., Frontera F., 2008, *ApJ*, 680, 602
- Fender R., 2006, in Lewin W. H. G., van der Klis M., eds, *Compact Stellar X-ray Sources*. Cambridge Univ. Press, Cambridge, p. 381
- Fender R. P., Homan J., Belloni T. M., 2009, *MNRAS*, 396, 1370
- Filippenko A. V., Chornock R., 2001, *IAU Circular*, 7644, 2
- Frontera F., Costa E., Dal Fiume D., Feroci M., Nicastro L., Orlandini M., Palazzi E., Zavattini G., 1997, *A&AS*, 122, 357
- Frontera F. et al., 2001, in Gimenez A., Reglero V., Winkler C., eds, *Exploring the Gamma-Ray Universe, ESA SP-459*. ESA, Noordwijk, p. 187
- Gandhi P. et al., 2011, *ApJ*, 740, L13
- Garnavich P., Quinn J., 2000, *IAU Circular*, 7388, 3
- Garnavich P. M., Stanek K. Z., Berlind P., 1999, *IAU Circular*, 7276, 1
- Gierliński M., Done C., Page K., 2008, *MNRAS*, 388, 753
- Hynes R. I., Haswell C. A., Chaty S., Shrader C. R., Cui W., 2002, *MNRAS*, 331, 169
- Hynes R. I. et al., 2006, *ApJ*, 651, 401
- Ingram A., Done C., 2011, *MNRAS*, 415, 2323
- Laurent P., Titarchuk L., 2007, *ApJ*, 656, 1056
- Laurent P., Rodríguez J., Wilms J., Cadotte Bel M., Pottschmidt K., Grinberg V., 2011, *Sci*, 332, 438
- Lin D., Remillard R. A., Homan J., 2007, *ApJ*, 667, 1073
- Liu Q. Z., van Paradijs J., van den Heuvel E. P. J., 2001, *A&A*, 368, 1021
- McClintock J. E., Remillard R. A., 2006, in Lewin W. H. G., van der Klis M., eds, *Compact Stellar X-ray Sources*. Cambridge Univ. Press, Cambridge, p. 157
- McCollough M. L., Wilson C. A., 1999, *IAU Circular*, 7282, 3
- Magdziarz P., Zdziarski A. A., 1995, *MNRAS*, 273, 837
- Malzac J., Merloni A., Fabian A. C., 2004, *MNRAS*, 351, 253
- Manzo G., Giarrusso S., Santangelo A., Ciralli F., Fazio G., Piraino S., Segreto A., 1997, *A&AS*, 122, 341
- Mitsuda K. et al., 1984, *PASJ*, 36, 741
- Montanari E., Titarchuk L., Frontera F., 2009, *ApJ*, 692, 1597 (M09)
- Morrison R., McCammon D., 1983, *ApJ*, 270, 119
- Parmar A. N. et al., 1997, *A&AS*, 122, 309
- Pooley G. G., Hjellming R. M., 1999, *IAU Circular*, 7278, 1
- Poutanen J., Svensson R., 1996, *ApJ*, 470, 249

- Press W. H., Teukolsky S. A., Vetterling W. T., Flannery B. P., 1992, *Numerical Recipes in C. The Art of Scientific Computing*. Cambridge Univ. Press, Cambridge, p. 609
- Protassov R., van Dyk D. A., Connors A., Kashyap V. L., Siemiginowska A., 2002, *ApJ*, 571, 545
- Remillard R. A., McClintock J. E., 2006, *ARA&A*, 44, 49
- Russell D. M., Fender R. P., Hynes R. I., Brocksopp C., Homan J., Jonker P. G., Buxton M. M., 2006, *MNRAS*, 371, 1334
- Sánchez-Fernández C., Castro-Tirado A. J., Giménez A., Zurita C., Casares J., Lund N., 2001, *Astrophys. Space Sci. Suppl.*, 276, 51
- Schnittman J. D., 2005, *ApJ*, 621, 940
- Schnittman J. D., Homan J., Miller J. M., 2006, *ApJ*, 642, 420
- Shakura N. I., Sunyaev R. A., 1973, *A&A*, 24, 337
- Shaposhnikov N., Titarchuk L., 2009, *ApJ*, 699, 453 (ST09)
- Stella L., Vietri M., 1998, *ApJ*, 492, L59
- Stella L., Vietri M., Morsink S. M., 1999, *ApJ*, 524, L63
- Tanaka Y., Shibazaki N., 1996, *ARA&A*, 34, 607
- Titarchuk L., 1994, *ApJ*, 434, 570
- Titarchuk L., Fiorito R., 2004, *ApJ*, 612, 988
- Titarchuk L., Osherovich V., 1999, *ApJ*, 518, L95
- Titarchuk L., Seifina E., 2009, *ApJ*, 706, 1463
- Titarchuk L., Mastichiadis A., Kylafis N. D., 1997, *ApJ*, 487, 834
- Titarchuk L., Shaposhnikov N., Arefiev V., 2007, *ApJ*, 660, 556
- Tomsick J. A. et al., 2003, *ApJ*, 597, L133
- Uemura M., Kato T., Pavlenko E., Shugarov S., Mitskevich M., Fried R. E., Sano Y., 2004, *PASJ*, 56, 147
- van der Klis M., 2000, *ARA&A*, 38, 717
- van Paradijs J., McClintock J. E., 1995, in Lewin W. H. G., van Paradijs J., van den Heuvel E. P. J., eds, *X-Ray Binaries*. Cambridge Univ. Press, Cambridge, p. 58
- Wagner R. M., Smith P. S., Schmidt G. D., Shrader C. R., 1999, *IAU Circular*, 7279, 1
- Wagoner R. V., Silbergleit A. S., Ortega-Rodríguez M., 2001, *ApJ*, 559, L25
- Wood A., Smith D. A., Marshall F. E., Swank J., 1999, *IAU Circular*, 7274, 1
- Zdziarski A. A., Gierliński M., 2004, *Progress Theor. Phys. Suppl.*, 155, 99
- Zurita C. et al., 2002, *MNRAS*, 334, 999

This paper has been typeset from a \LaTeX file prepared by the author.